Industrial Crops & Products 240 (2026) 122609

Contents lists available at ScienceDirect

Industrial Crops & Products

journal homepage: www.elsevier.com/locate/indcrop

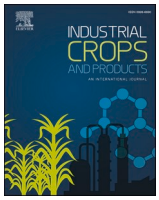

Ionic liquid functionalised nanoceria significantly enhances photosynthetic CO_2 sequestration

Leonard M. Kiirika [a], Mónia A.R. Martins [b], Dawid Perlikowski [a], Nicolas Schaeffer [c], Lakshmipathy Muthukrishnan [a], Suman Kalyan Sahoo [d], João A.P. Coutinho [c], Gregory Franklin [a,*], Dibyendu Mondal [a,d,**]

[a] Institute of Plant Genetics of the Polish Academy of Sciences, Strzeszyńska 34, Poznan 60-479, Poland
[b] CIMO, LA SusTEC, Instituto Politécnico de Bragança, Campus de Santa Apolónia, Bragança 5300-253, Portugal
[c] CICECO – Aveiro Institute of Materials, University of Aveiro, Aveiro 3810-193, Portugal
[d] Centre for Nano and Material Sciences, Jain (Deemed-to-be University), Jain Global Campus, Kanakapura, Bangalore, Karnataka 562112, India

ARTICLE INFO

Keywords:
Photosynthetic CO_2 fixation
Ionic liquid
Engineered nanomaterial
Nanoceria
Sustainable agriculture

ABSTRACT

The threat posed by increasing CO_2 concentrations in the atmosphere requires innovative carbon sequestration technologies. Photosynthetic CO_2 sequestration by plants is a sustainable pathway, but its full potential is limited due to CO_2 diffusion and abiotic stress in the plant. Engineered nanomaterials such as nanoceria (CeO_2) can increase the activity of chloroplasts due to their photocatalytic activity and thus stimulate photosynthetic processes. In the present study, the development of a new nanoformulation of CeO_2 whose surface was functionalised with an ionic liquid (IL), cholinium ascorbate ([Cho][Asc]) was investigated to enhance photosynthetic CO_2 fixation in tobacco plants. Compared to CeO_2 and IL, the CeO_2 + [Cho][Asc] nanoformulation significantly improved plant growth, biomass yield, photosynthetic rate and CO_2 fixation. Compared to the control, plants treated with CeO_2 + 50 mM [Cho][Asc] showed ~2-fold higher photosynthetic rate and a 198 % increase in dry biomass accumulation. The maximum quantum efficiency of photosystem II (F_v/F_m) results were consistent with the observed photosynthetic rate. Application of CeO_2 + 50 mM [Cho][Asc] resulted in CO_2 sequestration of 3.02 t/hectare, which is 80–110 % higher than CeO_2 and IL applied separately, and 279 % higher than the control. This improvement in photosynthetic CO_2 fixation was achieved without compromising tobacco seed yield, as foliar application of CeO_2 + 50 mM [Cho][Asc] resulted in significantly higher seed yield than in control plants. Overall, this study provides insights into the effects of IL-modified CeO_2-based nanoformulations on plant growth and CO_2 fixation, contributing to sustainable agriculture and mitigating climate change.

1. Introduction

The increasing accumulation of carbon dioxide (CO_2) in the atmosphere poses a serious threat to the climate, food supply and ecosystems (Shen et al., 2025). While carbon mineralisation and CO_2 fixation into platform chemicals are potential technological solutions (Sanna et al., 2014; Aresta et al., 2014), natural solutions such as photosynthetic CO_2 sequestration are crucial (Daneshvar et al., 2022; Peng et al., 2025). However, the inefficient conversion of solar energy in most crops (<2 %) limits CO_2 diffusion and restricts the ability of plants to sequester CO_2 efficiently Matthews (2023). Recent breakthroughs in nanotechnology offer an alternative to increase the CO_2 sequestration capacity of plants by enhancing photosynthesis (Giraldo et al., 2014; Liu et al., 2024; Chandra et al., 2014). Engineered nanomaterials (ENMs) can effectively interact with plants and modulate plant physiology, light absorption and biochemical pathways (Giraldo et al., 2014; Chandra et al., 2014). ENMs can contribute to CO_2 sequestration in crops and microalgae by catalysing the conversion of CO_2 into valuable products and supporting sustainable agriculture (Patel et al., 2025; Gan et al., 2014). Carbon-based nanostructures materials (Giraldo et al., 2014; Chandra et al., 2014), metal oxide nanoparticles (Wu et al., 2017), and semiconductor quantum dots (Liu et al., 2024), among other classes of ENMs (Jahani et al., 2019; Yan et al., 2025; Ze et al., 2011), have been shown to affect photosynthetic efficiency and carbon assimilation in both

* Corresponding author.
** Corresponding author at: Institute of Plant Genetics of the Polish Academy of Sciences, Strzeszyńska 34, Poznan 60-479, Poland.
E-mail addresses: fgre@igr.poznan.pl (G. Franklin), dmon@igr.poznan.pl, m.dibyendu@jainuniversity.ac.in (D. Mondal).

https://doi.org/10.1016/j.indcrop.2025.122609
Received 9 September 2025; Received in revised form 6 November 2025; Accepted 29 December 2025
Available online 6 January 2026

model and crop plant species. Metal oxide nanoparticles such as nanoceria (CeO_2) have photocatalytic properties that can stimulate light-harvesting ability under suboptimal conditions (Wu et al., 2017; Jahani et al., 2019; Abbas et al., 2020; Du et al., 2015). CeO_2 has also been used to inhibit the degeneration of chloroplasts and thus support their photosynthetic activity (Wu et al., 2017). CeO_2 acts as a cofactor for numerous enzymes and influences essential metabolic processes such as photosynthesis, respiration, antioxidant system and signal transduction (Gong et al., 2011). Despite these promising results, the use of such ENMs for photosynthetic CO_2 sequestration is still at an early stage. A comprehensive understanding of the interactions between nanomaterials and plants in photosynthetic CO_2 sequestration is essential.

The unique properties of ENMs, including size, shape, and surface charge, can be tailored to optimize their activity while controlling the release of metal ions, which is critical for improving their utilisation efficiency (Jiménez-Rosado et al., 2022; Ma et al.; 2020; Martins et al., 2024). Recently, we showed the potential of ionic liquids (ILs) for tailoring the release of copper ions from CuO nanoparticles to improve the use efficiency of CuO-based nanofertilizers (Martins et al., 2024). Several studies have investigated the effects of ILs, a well-known class of green solvents, on plant growth and development (Xia et al., 2018; Yu et al., 2018). The mechanism underlying these positive effects is believed to be the ability of ILs to solubilize nutrients and promote their uptake by plants. Recently, the application of di-cationic ILs was reported to exhibit growth-stimulating activity in corn plants, as evidenced by a significant increase in fresh weight and dry weight of corn cobs (Kaczmarek et al., 2023). However, the engineering of nanomaterials with ILs for sustainable and environmentally friendly photosynthetic CO_2 fixation has hardly been explored (Martins et al., 2024). The combination of ENMs with ILs not only improves their intrinsic properties but also enables controlled and targeted delivery mechanisms.

The present study explores the emerging potential of surface functionalisation of CeO_2 with IL, cholinium ascorbate ([Cho][Asc]), to enhance plant CO_2 capture by improving photosynthetic performance. The reason behind selecting CeO_2 is its known effect on photosynthesis by modulating stomatal opening (Wu et al., 2017). Cholinium ions are involved in membrane integrity, phospholipid metabolism and synthesis of plant growth regulators, which contributes to improved plant growth and ascorbate is well known antioxidant for stress resistance (Nuccio et al., 2000). Overall, the effects of CeO_2 and [Cho][Asc]-based nanoformulations on plant growth, photosynthetic performance and CO_2 fixation were investigated and compared with pure CeO_2 and pure IL treatments in *Nicotiana tabacum* (tobacco). Overall, the effect of IL-modified CeO_2-based nanoformulations on enhanced photosynthetic CO_2 fixation is demonstrated to promote sustainable agriculture and contribute to climate change mitigation.

2. Experimental methods

2.1. Materials

Choline bicarbonate (80 % w/w aqueous solution) and ascorbic acid (99.7 %) were procured from Sigma Aldrich. Both precursors were used directly to synthesize [Cho][Asc] IL, without further purification. Double distilled ultrapure water purified using a Milli-Q plus water (resistivity = 18.2 MΩ cm, total organic content < 5 μg dm^{-3}, particle-free > 0.22 μm) was employed. CeO_2 nanoparticles dispersed in water (CeO_2, 20 wt%, 30–50 nm, stock#: US7110, CeO_2 CAS# 1306–38–3, H_2O CAS# 7732–18–5) was procured from US Research Nanomaterials, Inc (USA), and freeze-dried before use. Analytical grade ethanol was acquired from Fisher Scientific, while dialysis tubing cellulose membranes were obtained from SIGMA (D9277).

2.2. Synthesis of IL

[Cho][Asc] was synthesised by neutralising cholinium bicarbonate with ascorbic acid (1:1 mol ratio), following the method described by Sharma et al. (2021). Briefly, ethanol was used to suspend the ascorbic acid, which was then added dropwise to an excess of base under vigorous stirring at room temperature, producing carbon dioxide and water. To remove the formed carbon dioxide, the mixture was stirred with the lid open and left to stand for 24 h. Unreacted starting materials were removed by liquid-liquid extraction with ethyl acetate (Sigma Aldrich). The synthetised IL was then dried under vacuum (1 Pa) with stirring at room temperature for 48 h.

2.3. Characterizations

The structural integrity of the IL was confirmed by ^{1}H NMR (Nuclear Magnetic Resonance) spectroscopy, in a Bruker Avance 300 at 75 MHz using deuterated water (D_2O) as solvent, which showed a 1:1 acid-base ratio and a purity higher than 97 %. In addition, CeO_2 was characterized before and after dissolution experiments and contact with ILs using scanning Transmission Electron Microscopy (TEM) and powder X-ray diffraction (p-XRD). For TEM analyses, nano-materials (NMs) were suspended in water, dispersed by sonication, and TEM grids were prepared by immersion. Measurements were conducted using a Hitachi HD-2700 microscope at 200 kV. p-XRD measurements were performed in diffraction-free sample holders at room conditions using an Empyrean X-ray diffractometer from PANalytical B.V. operating with a Cu anode (Kα1 = 1.5406 Å; Kα2 = 1.5444 Å) and equipped with a PIXcel^{1D} detector. Diffraction data were collected in continuous mode in the 2θ range of 10–70° in steps of 0.04° and with a time per step of 295 s. The UV–vis spectrophotometer (UV-1800, Shimadzu, Kyoto, Japan) of IL and CeO_2 and their combination were carried out in 200 nm to 800 nm wavelength range with a resolution of 1 nm. The particle size and zeta potential of IL, CeO_2, and IL+CeO_2 were determined using the dynamic light scattering spectrometer (DLS) Litesizer DLS 500 (Anton Paar, Austria).

2.4. Dissolution kinetics of Ce ions from CeO_2 in PGR-ILs

To determine the rate at which Ce ions are released from the CeO_2-based formulations, the dissolution kinetics was studied in ultrapure water and in aqueous solutions containing [Cho][Asc], following the procedure described previously (Martins et al., 2024). Briefly, dialysis membranes pretreated as per the recommendation of the manufacturer, were filled with water or water + [Cho][Asc], plus CeO_2 in excess. The systems were ultrasonicated for 2 min to disperse the particles and then shake at 200 rpm and 25°C using a Carousel 12 Plus reaction station. Aqueous samples of approximately 1 g were collected at different time points, diluted in 1 wt% polyvinyl alcohol, and added a known concentration of yttrium standard (1000 mg/L Certipur® standard, Sigma-Aldrich). 10 μL of each sample was then placed on a previously treated carrier (containing 10 μL of silicon in isopropanol solution) and dried on a hot plate at 353 K. The concentration of Ce ions was measured using a Picofox S2 total reflectance X-ray fluorescence spectrometer (TXRF) from Bruker Nano, USA, equipped with a molybdenum X-ray source (X-ray tube voltage: 50 kV and current: 600 μA). For each time point and solution, at least three independent measurements were performed, with an acquisition time of 500 s. For the preparation of suspensions, the initial concentration of CeO_2 was around 100 ppm, while the concentration of [Cho][Asc] was 12 mM. The pH of the suspensions was measured both before the experiment (in aqueous solutions of [Cho][Asc]) and after its completion (in aqueous solutions of [Cho][Asc] and dissolved cerium ions), using a Mettler Toledo™ S470 benchtop pH meter.

2.5. Effects of CeO_2+ [Cho][Asc] nanoformulations on tobacco plants

To study the effects of nanoformulations on tobacco plant growth, treatments were prepared as follows: (1) H_2O, (2) H_2O + CeO_2, (3) H_2O + CeO_2 + [Cho][Asc:1 mM], (4) H_2O + CeO_2 + [Cho][Asc:10 mM], (5) H_2O + CeO_2 + [Cho][Asc:50 mM], and (6) H_2O + [Cho][Asc:10 mM]. A suspension containing CeO_2 and/or [Cho][Asc] ILs was concocted by mixing 100 ppm of CeO_2 in specified quantities with ultrapure water in Falcon tubes. The mixture underwent sonication for 5 min and was left to stir at 100 rpm for 7 days under standard room temperature conditions. The formulation containing both dissolved and undissolved CeO_2 along with IL was used without any filtration step for foliar application and the same solution was used throughout the experiment. The formulation was foliar applied on tobacco plants *(N. tabacum* Petit Havana L. CV) grown under controlled greenhouse condition, 19 days after transplanting. In brief, seeds were sterilised for 1 min with 70 % ethanol (v/v), followed by a triple wash with sterile deionised H_2O. Subsequently, they were soaked in 50 % (v/v) sodium hypochlorite with an active chlorine concentration of 1.5 % for 6 min, followed by another triple rinse in sterile deionized H_2O. Seeds were germinated on half-strength Murashige and Skoog (1962) culture media supplemented with sucrose (15 g/L). Tobacco seedlings were then planted in pots with sterile peat substrate and maintained under greenhouse conditions (16/8 light/dark cycle, light intensity 90 μmol m^{-2} s^{-1}, 70 % RH, and temperature 24°C). The experiment followed a completely randomized design (CRD) with three replicates. Seedlings received five applications of CeO_2 + IL -based nanoformulations at one-week intervals until the end of the experiment. Each pot received approximately 1 g of the nanoformulations per treatment. The control plants were treated with ultrapure water without any nanoformulations. Prior to application, plants were checked for uniformity, well-developed shoots, and differentiated leaves. Pots were consistently watered to field capacity (3.5 mL/g substrate) during the experiment. Plant performance was assessed weekly after each foliar application, at the following time points: 0, 7, 14, 21, 28, and 35 days post-treatment. At every interval, plant height (net plant length) was measured from the base of the stem to the apex using a precision ruler. At the end of physiological data collection (5 weeks after transplanting), destructive harvest was performed to obtain fresh and dry biomass data. Plants were carefully uprooted, and roots and shoots were separated and carefully washed with tap water, followed by distilled water. Excess surface moisture was removed using sterile filter paper before determining the fresh weight with an analytical balance. Samples were then oven-dried at 65°C for 48 h in a forced-air drying oven to obtain dry weight measurements, providing a robust estimation of biomass accumulation across treatments. Phenotypic data were systematically collected in triplicate for each treatment, and images of both plant shoots and roots were captured to qualitatively assess the effects of the treatments. Pod length and diameter were measured using a digital calliper. Pods were air-dried to determine dry weight, and seeds were manually separated for dry weight determination and counted using an electronic seed counter. All measurements were performed in triplicate to ensure accuracy and statistical reliability.

2.6. Effects of CeO_2+ [Cho][Asc] nanoformulations on leaf gas exchange and photosynthesis

The leaf chlorophyll index was studied non-destructively by measuring the leaves of tobacco plants using a portable SPAD-502Plus Chlorophyll Meter (Konica Minolta GmbH) at 14th and 21st days post treatment (dpt). To study the effects of CeO_2+ [Cho][Asc] nanoformulations on leaf gas exchange and photosynthesis, the leaf photosynthetic efficiency was measured on individual plants per treatment and sampling point (14-dpt), and at each foliar spray. Photosynthetic parameters were measured in triplicates for every plant considering actively growing leaves, with 9 measurements per treatment. Gas exchange parameters such as net photosynthetic rate P_N (μmol CO_2 m^{-2} s^{-1}), transpiration *Tr* (mmol H_2O m^{-2} s^{-1}), conductance Cond (mol H_2O m^{-2} s^{-1}), and intercellular CO_2 concentration Ci (μmol CO_2 mol^{-1}) were measured using a LI-6400XTPortable Photosynthesis System (LI-COR Biosciences) on a leaf in the same position on every plant. Measurements were made under artificial light conditions in the chamber at an intensity of 750 μmol m^{-2} s^{-1}, 400 μmol mol^{-1} CO_2 with a flux of 200 μmol 217 s^{-1}, and 50–65 % RH. The instrument was recalibrated after every measurement of 15 samples to obtain stable readings.

The leaf chlorophyll fluorescence assessments were conducted using a chlorophyll fluorescence analyser (OS1p, Opti-Sciences, Hudson, NH) according to Rossi et al. (2016). Briefly, healthy tobacco leaves were selected on the plant considering 5 plants per treatment. Prior to measurements, leaves were adjusted to dark for 30 min according to Maxwell and Johnson (2000). Fluorescence parameters considering the baseline (F_0) and maximum (F_m) fluorescence were quantified, and subsequent calculations involved the derivation of variable fluorescence ($F_v = F_m - F_0$) and the ratio of variable fluorescence to maximum fluorescence (F_v/F_m).

2.7. Effects of nanoformulations on CO_2 sequestration

To assess the CO_2 sequestration in the plant, carbon content was estimated using a CHNS analyzer (Leco Truspec-Micro CHNS 630–200 200). The leaves, root and shoot tissues were ground into a fine powder using a homogenizer (Taurus, 25 790 Barcelona, Spain) and passed through a 1 mm mesh sieve. The carbon content in the root and shoot tissues, along with dry biomass yield, was used to estimate CO_2 sequestration (Martins et al., 2024).

2.8. Computational details

The geometry optimization of $Ce_{10}O_{20}$ cluster, the adsorption study of [Cho][Asc] ionic liquid with water molecule, and cerium leaching studies were performed by density functional theory (DFT) methods as implemented in Vienna Ab initio Simulation Package (VASP) code (Kresse and Furthmüller, 1996). The electron–ion interaction was defined using the projector augmented wave (PAW) pseudopotential method (Blöchl, 1994; Kresse and Joubert, 1999). The spin-polarized Perdew-Burke-Ernzerhof (PBE) functional within the generalized gradient approximation (GGA) was used to compute the exchange–correlation energy (Perdew et al., 1996). All simulations used a plane-wave basis set with a fixed energy cutoff of 400 eV. Geometry optimisations were performed via ionic relaxation using the conjugate gradient method. The geometries were considered converged when the force tolerance was 0.02 eV $Å^{-1}$ and the energy tolerance was 10^{-5} eV. The atomic structures were visualized by VESTA code (Momma and Izumi, 2008). The adsorption energy of molecule on CeO_2 cluster obtained by the equation $Eads = Emolecule@cluster - (Ecluster + Emolecule)$, where *Ecluster*, *Emolecule* and *Emolecule@cluster* are the energies of the CeO_2 cluster, adsorbed molecule and the entire composite system (molecule@cluster), respectively. The cerium ion leaching studies are modeled by the removing one cerium atom from the $Ce_{10}O_{20}$-ionic liquid-water composite system.

2.9. Statistical analysis

All data were statistically analysed using one-way ANOVA ($p < 0.05$) to determine significant differences between treatments. Post-hoc comparisons between treatments were performed using the independent samples *t*-test, followed by Duncan's multiple range test.

3. Results and discussion

3.1. Surface functionalisation of nanoceria with ionic liquid

Fig. 1a shows the schematic representation of the protocol adopted for the surface engineering of CeO_2 with an aqueous solution of [Cho][Asc]. After 7 days of continuous stirring of 100 ppm CeO_2 in 50 mM [Cho][Asc], the mixture was characterized by various analytical methods.

The crystalline structure of CeO_2 with a crystallite size of 28.2 nm was confirmed by p-XRD analysis (Fig. 1b). The diffraction peaks correspond to the characteristic Bragg reflections of CeO_2, which are assigned to the planes (111), (200), (220), (311) and (222). No changes or shifts in X-ray diffraction angles were observed for CeO_2 when exposed to the IL-based medium, suggesting that [Cho][Asc] does not affect the morphology or crystallinity of CeO_2. The UV-Vis spectrum of CeO_2 shows an absorption peak at 317 nm (Fig. 1c), which is due to the charge transfer from the oxygen 2p valence band to the cerium 4 f conduction band (Safat et al., 2021). This peak remains unchanged after treatment with IL, suggesting that the morphology and size of CeO_2 do not change after functionalization with IL. The absorption maxima at 266 nm in [Cho][Asc] and CeO_2+ [Cho][Asc] are due to the π-π* transition of $[Asc]^-$ (Witmer et al., 2016). The DLS results show that the hydrodynamic diameters of [Cho][Asc] and CeO_2 + [Cho][Asc] are similar (Fig. 1d), which is consistent with the p-XRD and UV–vis analysis. However, the hydrodynamic radius is over 4 times the crystallite size which is also coherent with the TEM (Fig. 3a), suggesting partial aggregation of the particles in solutions. The zeta potential of CeO_2 was measured to be −47.2 mV (Fig. 1e). However, after engineering with IL, the surface charge decreased to −34.6 mV, confirming the successful surface functionalization of CeO_2 with IL. The interplay between nanoceria, water molecules, and [Cho][Asc] IL was examined through DFT-based simulations considering a cluster based model for ceria nanoparticle. The initial geometry of the $Ce_{10}O_{20}$ cluster was adopted based on results from a global structural optimization study (Zibordi-Besse et al., 2018). The optimized structures of $Ce_{10}O_{20}$ cluster, [Cho][Asc], and [Cho][Asc] + $Ce_{10}O_{20}$ cluster composite systems are given in Fig. 2. The calculated adsorption energy of the [Cho][Asc] on $Ce_{10}O_{20}$ cluster is −0.28 eV, confirming a favourable thermodynamic binding, which allow facile surface functionalization of the IL on nanoceria.

To investigate the morphology and composition of CeO_2, which may directly affect its dissolution and subsequent accumulation in plants, the characterization of CeO_2 was performed by TEM (Figs. 3a-3b). The corresponding EDS spectra of CeO_2 before and after 7-day exposure to [Cho][Asc] can be found in Fig. S1. The TEM image of the original CeO_2 at t_0 shows well-defined nanoparticles with minimal aggregation, quite similar to that after 7-day exposure to [Cho][Asc] (t_7), suggesting that the ILs do not affect the morphology and size of CeO_2 in aqueous solution of IL. The EDS spectra confirm the chemical composition of the materials and show that CeO_2 remains pure both before and after exposure to [Cho][Asc] (Fig. S1).

3.2. Release of cerium from ionic liquid functionalised nanoceria

The release of Ce ions from CeO_2 is a crucial process that ensures their long-term effectiveness. When ILs are added, the resulting nanoformulation is expected to exhibit controlled release properties and affect the availability of Ce ions over time. Dialysis tubes with cellulose membranes were used to evaluate the release profiles of Ce ions using

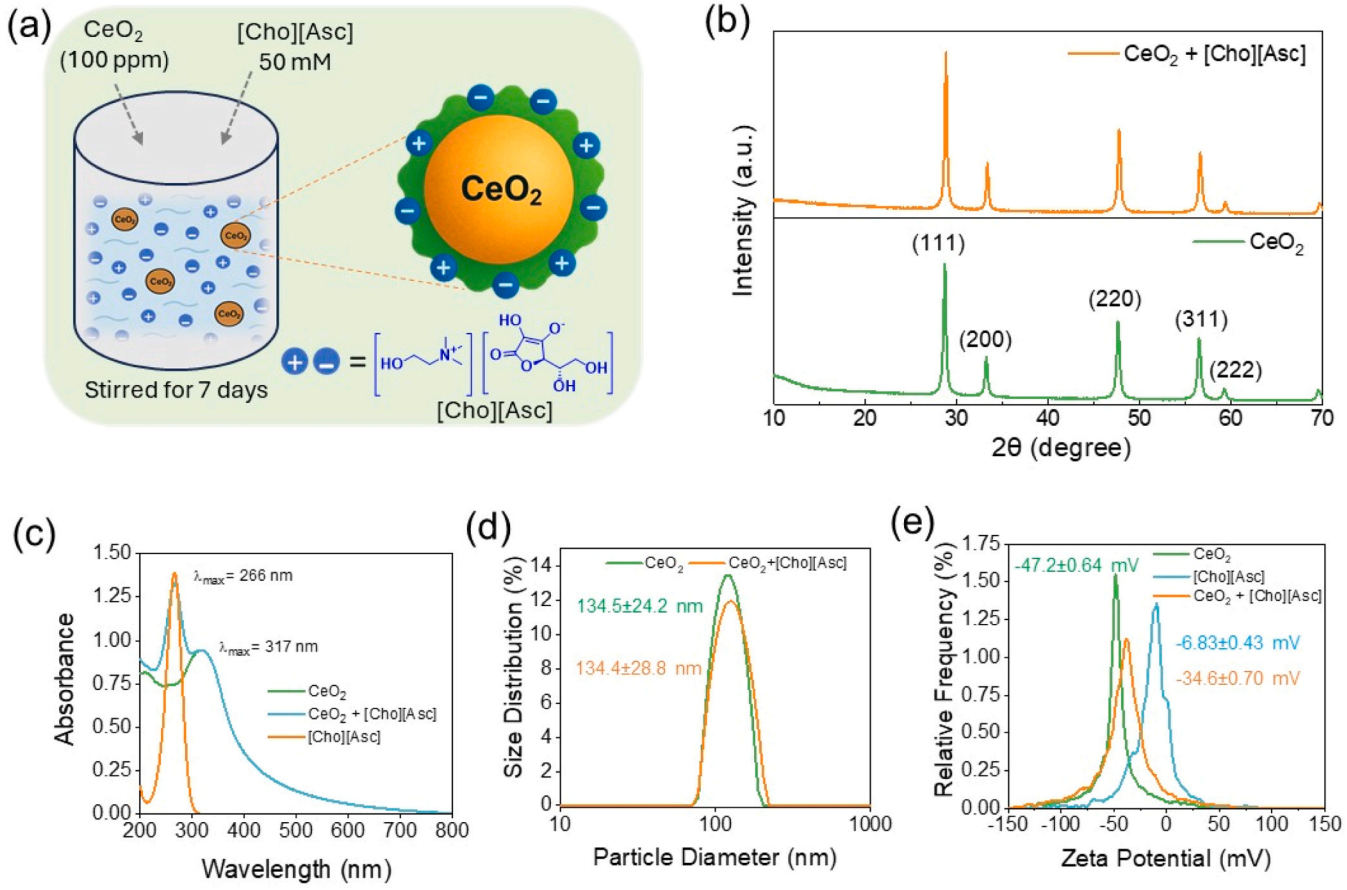

Fig. 1. (a) Schematic representation of surface engineering of CeO_2 with IL, [Cho][Asc]. (b) p-XRD, (C) UV–vis spectra, (d) DLS plot, and (e) zeta potential of CeO_2 nanoparticles before and after 7 days of exposure to the [Cho][Asc]-based medium.

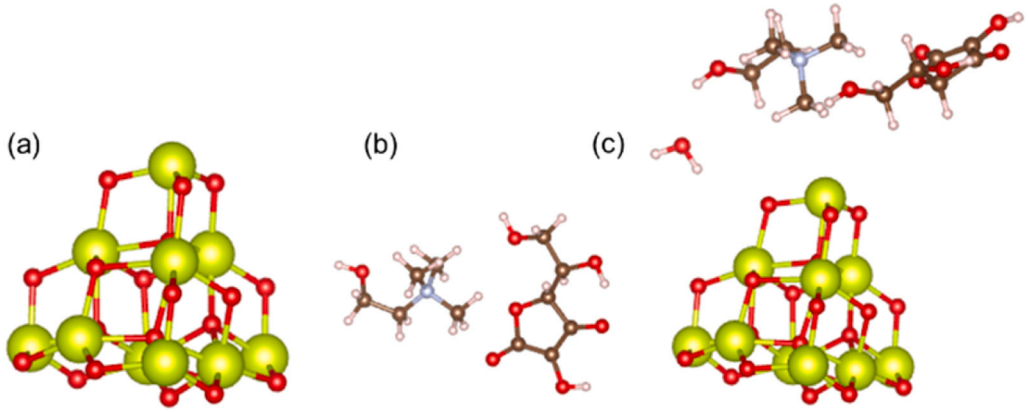

Fig. 2. Optimized structure of (a) $Ce_{10}O_{20}$ cluster, (b) [Cho][Asc] ionic liquid, and (c) [Cho][Asc] and H_2O functionalized $Ce_{10}O_{20}$ cluster.

the methodology described previously and detailed in Section 2.4 (Martins et al., 2024). The dissolution of cerium was characterized by a continuous release of particles over the evaluation period of 35 days, which is accurately described by a second-order polynomial equation as shown in Fig. 3c. This model does not assume a final equilibrium concentration. The dissolution kinetics of CeO_2 in pure water was also studied over a period of 7 days, but the values obtained were below the detection limit of the TXRF device.

We also calculated the energetics for cerium release tendency from the $Ce_{10}O_{20}$-water, $Ce_{10}O_{20}$-ionic liquid-water composite systems using DFT study (Fig. 3d-e). The calculations reveal that leaching is highly endothermic in both environments (+19.08 eV for H_2O-Ce_9O_{20} cluster and +17.04 eV for[Cho][Asc][H_2O]-Ce_9O_{20} cluster), however the ionic liquid environment offers a more favourable release pathway than the $Ce_{10}O_{20}$–water system. These findings are consistent with our experimental observations, which show that the cerium concentration in solution remains very low during the first two days of the release experiment (Fig. 3c"). After 7 and 35 days, the dissolution of CeO_2 + [Cho][Asc] in water was 171 and 1322 μg/L, respectively, showing that time significantly affects the leaching of cerium compared to water alone. In addition, the pH values of the solutions were measured before and after exposure to [Cho][Asc]. The pH of the [Cho][Asc] solution remained unchanged at 4.8 before and 7 days after the addition of CeO_2, with the slightly acidic nature promoting ion dissolution.

3.3. *Effect of ionic liquid functionalised nanoceria on plant growth*

Following the successful production of IL-functionalized CeO_2, a study was conducted to investigate its potential to improve the phenotypic and physiological properties of tobacco plants. Normally, nanoceria can interact with mesophyll cell walls and plasma mebranes and promote redox reactions that increase photosynthetic efficiency (Wu et al., 2017). However, at high concentrations, they can lead to oxidative stress, damage choloplasts, and decrease chlorophyll content (Du et al., 2015). On the other hand, $[Asc]^-$ is a potent antioxidant that can neutralize oxidative stress. This suggests that the combination of [Cho][Asc] with nanoceria could lead to a balanced generation of reactive oxygen species (ROS), which would be beneficial for plant performance. To understand the effects of IL modification of CeO_2 on plant growth, a control study was conducted with at a similar concentration without CeO_2. A total of six treatments (1:H_2O, 2: H_2O + CeO_2, 3: H_2O + CeO_2 + [Cho][Asc:1 mM], 4: H_2O + CeO_2 + [Cho][Asc:10 mM], 5: H_2O + CeO_2 + [Cho][Asc:50 mM], and 6: H_2O + [Cho][Asc:10 mM]) were prepared using combinations of CeO_2 (100 ppm) and different concentrations of [Cho][Asc]. It is important to note that the formulation contains both dissolved and undissolved CeO_2, along with IL, because no filtration step is performed before application (Section 2.5). The tobacco seedlings received five applications of the nanoformulations at one-week intervals until the end of the experiment. Growth and physiological responses of the plants were evaluated at 0, 7, 14, 21, 28 and 35 days after treatment. A detailed protocol for the evaluation of the growth parameters can be found in (Section 2.5). Fig. 4a shows the images of tobacco plants harvested after 35 days of cultivation. A visible difference was observed in the treatment with IL+CeO_2 compared to the control and treatments with IL and CeO_2 separately. Plants treated with CeO_2 + 50 mM [Cho][Asc] ILs stand out from all other treatments. A continuous growth assesment over 5 weeks showed that after that time there was a significant increase in plant height in both the plants treated with CeO_2 + 10 mM [Cho][Asc] and those treated with CeO_2 + 50 mM [Cho][Asc] (Fig. S2). The plants treated with CeO_2 + 50 mM IL showed a 59 % and 48 % higher plant height than the control and the plants treated with CeO_2 alone, respectively (Fig. 4b). This significantly higher plant height also resulted in higher shoot and root biomass production of the IL-modified CeO_2-treated plants. In addition, a clear dose-response relationship was observed, with the highest concentration (50 mM) resulting in the highest growth performance. Specifically, plants treated with CeO_2 + 50 mM [Cho][Asc] IL showed an increase in fresh biomass by 108 %, 51 % and 34 % compared to sprayed with H_2O, CeO_2 and IL, respectively (Fig. 4c). A similar trend was observed in dry biomass yield, where treatment with CeO_2 + 50 mM [Cho][Asc] IL resulted in 198 %, 106 % and 70 % higher dry biomass production compared to the plants sprayed with H_2O, CeO_2 and IL, respectively (Fig. 4d).

Previous studies have shown that the application of CeO_2 nanoparticles improved the biomass productivity of *Brassica napus* (canola) (Rossi et al., 2016), and enhanced overall yield, fruit quality, and postharvest storage of tomatoes (Feng et al., 2022). Ahmad et al., (2025) showed that foliar application of CeO_2 nanoparticles combined with biochar improved nutrient uptake under stress and led to enhanced growth and yield of rice. Engineered for controlled nutrient release, CeO_2 nanoparticles have the capacity to ensure a consistent nutrient supply and promote sustainable plant growth (Servin and White, 2016). Thus, the application of CeO_2 + [Cho][Asc] ILs may have synergistically interacted with the intrinsic cell structure of the plants, possibly stimulating growth-related processes and improving nutrient uptake. The significantly higher dry biomass yield indicates the potential of the IL-functionalized CeO_2 to improve not only plant growth and biomass production, but also water use efficiency. Overall, comparison with a control group shows a remarkable increase in plant growth and biomass production of plants treated with CeO_2 + [Cho][Asc] ILs, confirming the suitability of IL-modified CeO_2 as a stimulant for plant growth.

3.4. *Effect of ionic liquid functionalised nanoceria on photosynthetic parameters*

After the effects of IL-modified CeO_2 on growth promotion of tobacco plants were demonstrated, a comprehensive study was conducted to

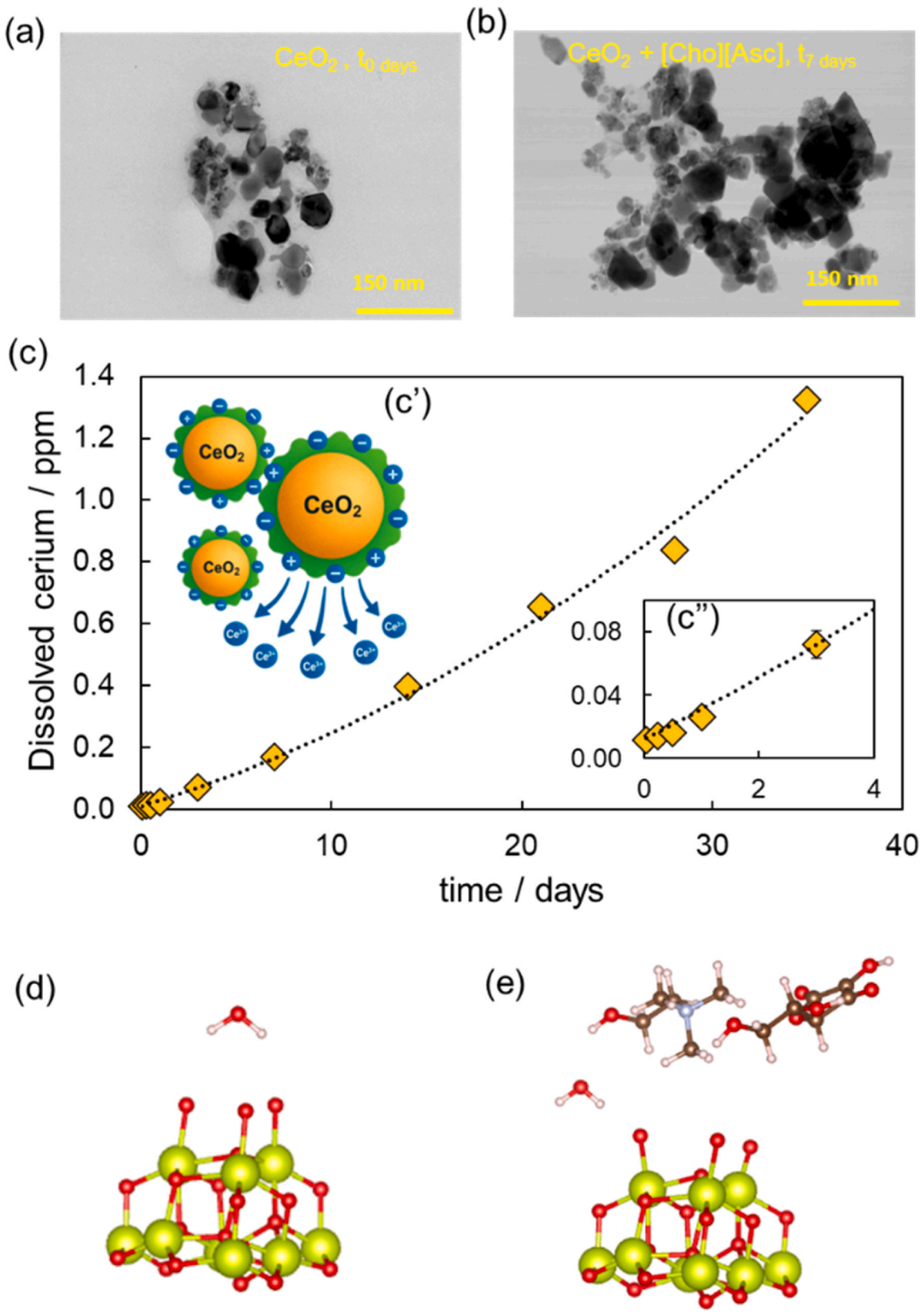

Fig. 3. (a-b) TEM micrographs of CeO_2 before and after 7 days of exposure to the [Cho][Asc] aqueous solution. (c) Dissolution kinetics of Ce ions in an aqueous solution of [Cho][Asc] at 25 °C and at an initial mass concentration of 100 ppm and 12 mM for CeO_2 and [Cho][Asc], respectively. Data were fitted to a second-order polynomial equation: Ce (ppm) $= 0.0005 \times t(days)^2 + 0.0185 \times t(days) + 0.0121$, $R^2 = 0.9938$. The insets showing the schematics of Ce^{3+} ions release (c') and initial 4 days dissolution data of Ce^{3+} (c''). (d) H_2O-Ce_9O_{20} cluster after release of one Ce ion. (e) [Cho][Asc][H_2O]-Ce_9O_{20} cluster after release of one Ce ion.

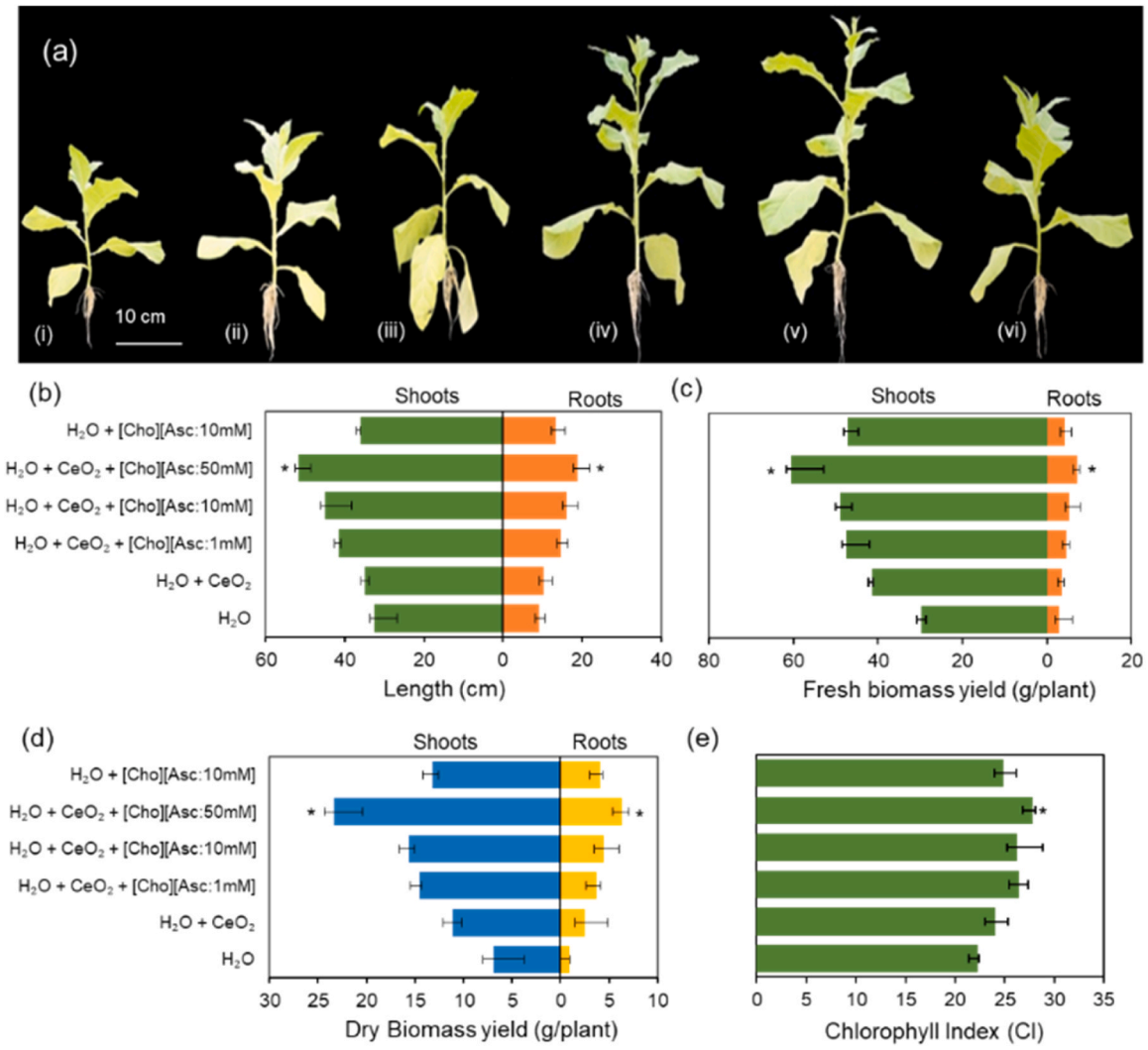

Fig. 4. (a) Images of tobacco plants treated with: (i) H_2O (control), (ii) $H_2O + CeO_2$, (iii) $H_2O + CeO_2$ + [Cho][Asc:1 mM], (iv) $H_2O + CeO_2$ + [Cho][Asc:10 mM], (v) $H_2O + CeO_2$ + [Cho][Asc:50 mM], and (vi) H_2O + [Cho][Asc:10 mM], taken 35 days after treatment. (b) Bar graph of mean values depicting plant length of treated tobacco plants. Effects of different treatments on the fresh biomass (c), dry biomass weights (d), and chlorophyll index (e) of tobacco plants. The error bars represent the standard error of the mean (SEM). The highly significant groups at a $p < 0.05$, in comparison to the control are indicated by asterisks (*).

investigate their photosynthetic performance. The detailed protocol for measuring various photosynthetic parameters can be found in Section 2.6. Photosynthesis is an essential plant process in which light energy is converted into chemical energy, which is crucial for plant growth and development. Chlorophyll is the most important pigment involved in photosynthesis and its content serves as an indicator of the rate of photosynthesis. The treatment combinations with different concentrations of [Cho][Asc] + CeO_2 showed a significant increase in the chlorophyll index of tobacco plants (Fig. 4e). The chlorophyll index increased with increasing IL concentration and showed a dose-response relationship. Overall, a 25–30 % increase in chlorophyll index was observed in plants treated with CeO_2 + 50 mM [Cho][Asc] compared to H_2O, CeO_2 and [Cho][Asc]. This increase in chlorophyll index indicates a higher photosynthetic rate (P_N) in the CeO_2 + [Cho][Asc] treatment.

Fig. 5 shows the physiological responses of tobacco plants to the treatments. A concentration-dependent pattern can be seen, indicating that CeO_2 + 50 mM [Cho][Asc] is an optimal concentration that significantly improves the physiological performance of the plants. As shown in Fig. 5a, a 176 % increase in P_N was observed in CeO_2-treated plants compared to the control, confirming the results of a previous report (Wu et al., 2017). A similar result was obtained for [Cho][Asc]-treated plants with a 168 % increase in P_N. However, a significantly higher P_N value (264 %) was obtained in the plants treated with CeO_2 + 50 mM [Cho][Asc] IL compared to the control, confirming the cooperative effect of the IL-functionalized CeO_2 nanoformulation on the photosynthetic rate. The observed P_N values reflect the trend of plant height and biomass yield (Figs. 4a-4d), suggesting that the improved plant growth is due to the increased photosynthetic efficiency. Foliar application of IL-modified CeO_2 nanoformulation could stabilize the ultrastructure of chloroplasts and mitochondria and help plants maintain their photosynthetic efficiency. In addition, a 2-fold increase in photosynthetic rate and an approximately 2-fold increase in dry biomass production suggest a synergistic effect of CeO_2 and [Cho][Asc] in buffering ROS generation, thereby enhancing the conversion of solar energy into chemical energy in the form of photosynthates. ENM- induced abiotic stress has been shown to affect the primary physiological response, namely stomatal closure, resulting in reduced CO_2 diffusion, decreased photosynthesis and impaired plant growth (Lowry et al., 2019). Foliar application of CeO_2 nanoparticles at a concentration of 100 mg/kg led to an increase in P_N, stomatal conductance, and leaf transpiration rate in spianch (Ahmad et al., 2024), even under elevated CO_2 concentration. In this study, intercellular CO_2 concentration was increased (17 %), stomatal conductance was higher (92 %) and leaf transpiration was higher (70 %) in plants sprayed with CeO_2 + 50 mM

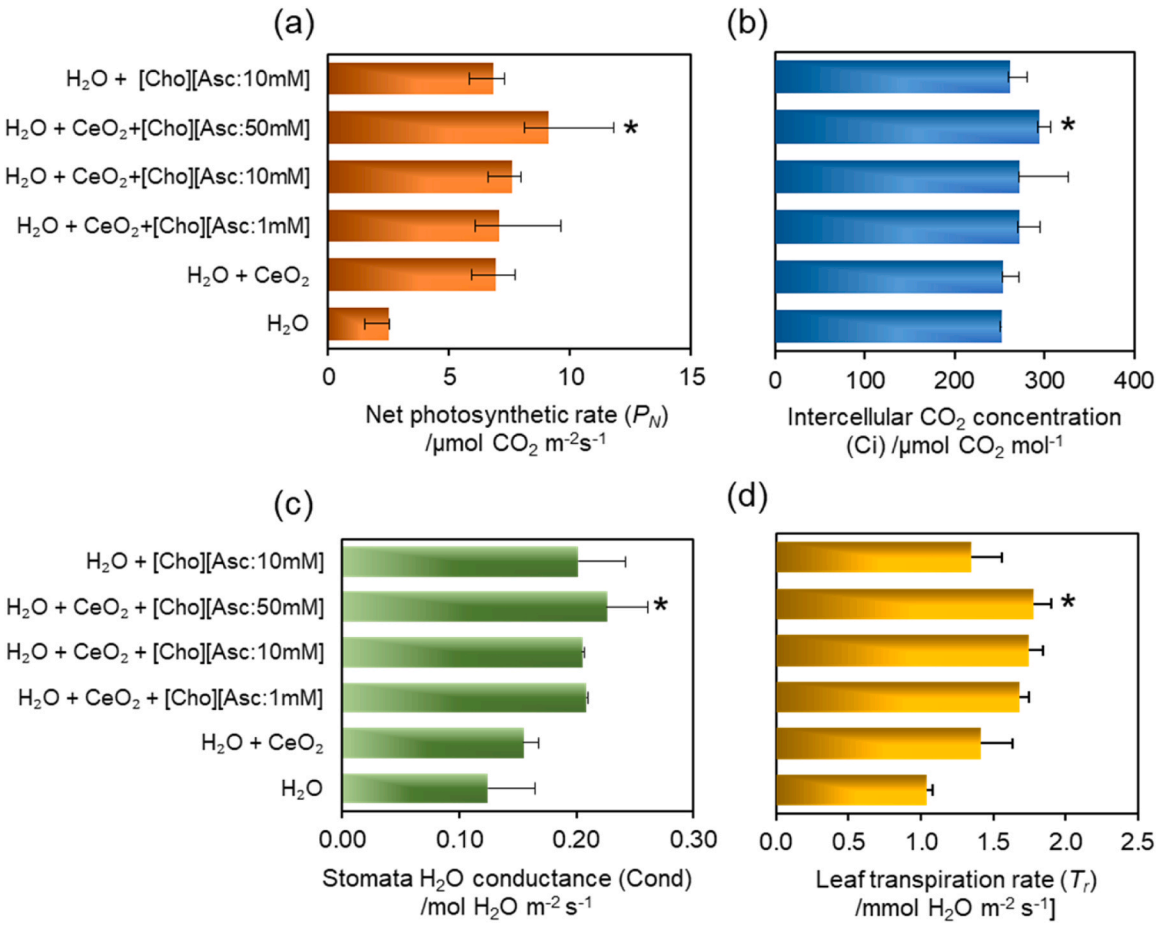

Fig. 5. Effects of CeO_2 + [Cho][Asc]ILs at three varying concentrations on (a) net photosynthetic rate, (b) intercellular CO_2 concentration, (c) stomatal H_2O conductance, and (d) leaf transpiration rate. The error bars associated with each column represent the standard error of the mean (SEM), and highly significant groups at a $p < 0.05$, in comparison to the control are indicated by asterisks (*).

[Cho][Asc] formulation (Figs. 5b-5d), indicating an effect of the treatments on plant physiological processes and the observed higher photosynthesis.

Fig. 6a shows the chlorophyll fluorescence of plants subjected to different treatments. The maximum quantum efficiency of photosystem II (F_v/F_m: the ratio of variable fluorescence to maximum fluorescence) is used to determine the photosynthetic health of a plant. It provides an indication of the maximum photochemical efficiency of PS II in the chloroplasts (Rossi et al., 2016). This parameter is proving valuable for assessing plant health, with the optimum F_v/F_m range typically between 0.79 and 0.84 in many plant species, with lower values indicating increased levels of plant stress (Rossi et al., 2016). To understand plant responses to the application of CeO_2 + [Cho][Asc] IL, a high-performance chlorophyll fluorescence analyser was used to quantify and analyse the intensity of fluorescent signals emanating from the leaves (Section 2.6). Tobacco plants were assessed 5 weeks after foliar application of CeO_2, [Cho][Asc] and CeO_2 + [Cho][Asc] IL. The determination of F_v/F_m showed a significant ($p < 0.05$) progressive increase in growth 1 week after treatment (Fig. 6a). Within 7 days of treatment with CeO_2 + 50 mM [Cho][Asc] IL, a significant increase in F_v/F_m of 3.1 was observed compared to control, and F_v/F_m increased up to 5 % after 35 days. This continuous increase in F_v/F_m between 0.79 and 0.83 indicates that the plants treated with CeO_2 + 50 mM [Cho][Asc] IL were exposed to less stress and showed good plant health throughout the experiment.

3.5. *Effect of ionic liquid functionalised nanoceria on photosynthetic CO_2 sequestration*

The observed increase in F_v/F_m, photosynthetic rate and growth performance in the IL modified CeO_2 treated plants could lead to higher photosynthetic carbon assimilation, which in turn contributes to photosynthetic CO_2 fixation. Accordingly, the effect of CeO_2 + [Cho][Asc] nanoformulation on photosynthetic CO_2 fixation was calculated as we reported before (Martins et al., 2024). Fig. 6b shows the amount of fixed CO_2 per plant after treatment with different nanoformulations in tobacco plants. As can be seen in Fig. 6b, the results of CO_2 sequestration follow the similar trends of photosynthesis rate (Fig. 5a). Compared to the control, an 80 % increase in CO_2 sequestration was observed in CeO_2-treated plants. Similarly, a 112 % increase in CO_2 sequestration was observed in the plants treated with [Cho][Asc] compared to the control. Remarkably, treatment of modified CeO_2 with [Cho][Asc] IL resulted in 279 % higher CO_2 sequestration compared to the control, confirming the synergistic effect of IL-modified CeO_2 nanoformulation in CO_2 sequestration. In a plant population of 75,000 plants/hectare of tobacco cultivation, foliar application of CeO_2 + 50 mM [Cho][Asc] would sequester 3.02 tons of CO_2, which is 80–110 % higher than foliar application of CeO_2 and IL formulation alone. In general, approximately 55–68 tonnes of CO_2 are sequestered per hectare annually through microalgal cultivation, and this could be further augmented by expousre to CeO_2 nanoparticles (Liu et al., 2024). Thus, the impact of IL-modified nanoceria on CO_2 sequestration could be more beneficial for improving microalgal biomass production via enhanced CO_2 fixation.

Furthermore, to assess the commercial potential of the IL-

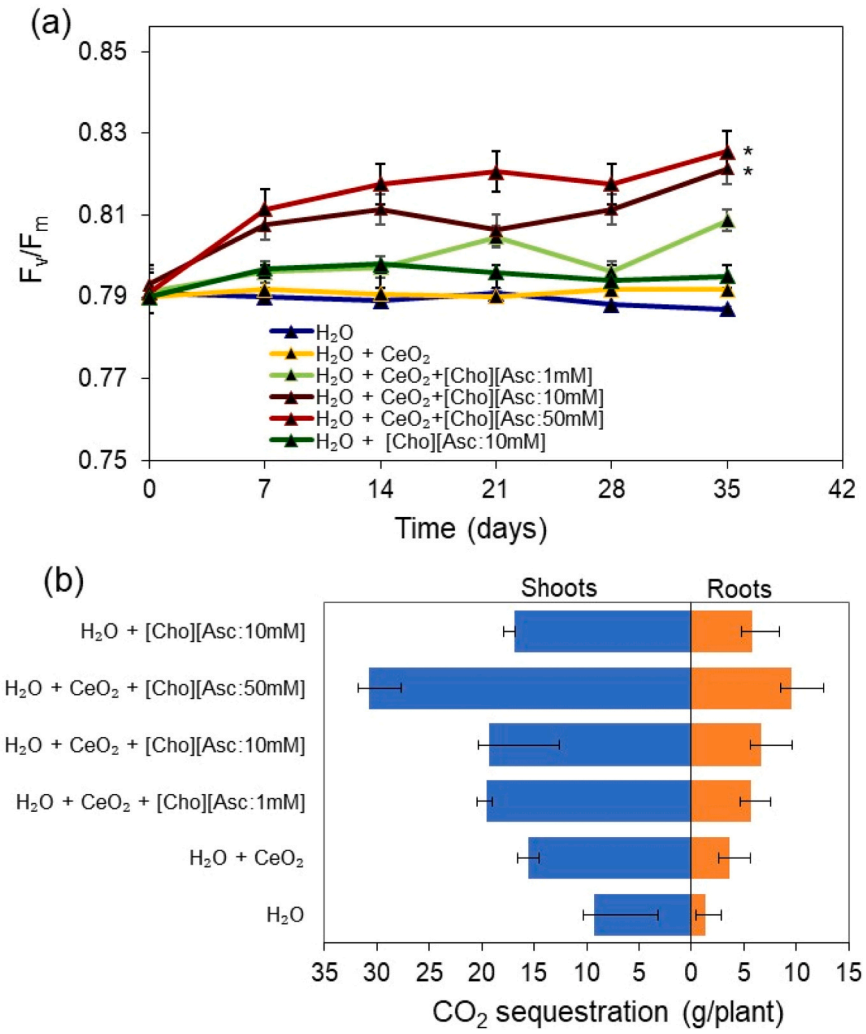

Fig. 6. (a) The maximum quantum efficiency of photosystem II (F_v/F_m) in tobacco leaves over a period of 35 days, assessed periodically at 7 days intervals after every treatment application. Highly significant groups at a $p < 0.05$, in comparison to the control are indicated by asterisks (*). (b) Effect of different treatments on the CO_2 sequestration.

functionalised CeO_2 nanoformulation in improving tobacco seed yield, we evaluated the yield parameters of tobacco seeds (Fig. 7). The results showed that pod size, number of pods per plant, and number of seeds per pod were all significantly higher in plants treated with CeO_2 + 50 mM [Cho][Asc] compared to the control (Fig. 7a-c). Although the weight of 100 seeds was similar to that of the control (Fig. 7d), the substantially higher number of pods per plant (52.4 % increase) and seeds per pod (44 % increase) in CeO_2 + 50 mM [Cho][Asc] treated plants indicate that the overall seed yield would be considerably greater than that of the control. Overall, the observed CeO_2 dissolution results (Fig. 3c), improved biomass yield (Fig. 4d), enhanced photosynthetic rate (Fig. 5a), higher F_v/F_m (Fig. 6a), heightened CO_2 sequestration (Fig. 6b), and enhanced seeds yield (Fig. 7) suggest that the impact of the nanoformulation is not governed by CeO_2 dissolution solely. The results reflect a combined effect of several factors which includes controlled ROS generation, modulation of stomatal opening and closing, enhanced nutrient uptake, and mitigation of abiotic stress.

4. Conclusions

A facile strategy to prepare an innovative nanoformulation by surface engineering of nanoceria with [Cho][Asc] IL was developed. The effects of the IL-modified CeO_2 nanoformulations on promoting plant growth, enhancing CO_2 sequestration, increasing the photosynthetic rate of tobacco plants, and improving seed yield were demonstrated. Foliar application of CeO_2+ [Cho][Asc] nanoformulation significantly promoted plant phenotypic growth, physiological aspects, and seeds yield in concentration-dependent responses. Compared with the control, pristine CeO_2 and [Cho][Asc] treatments, CeO_2+ [Cho][Asc]-treated plants showed a significant increase in plant height, photosynthetic efficiency, CO_2 sequestration, leaf chlorophyll fluorescence, biomass yield, maximum quantum efficiency of photosystem II (F_v/F_m), and tobacco seeds yield. The most notable result was a 2-fold increase in biomass productivity and photosynthetic rate, and a 2.8-fold increase in CO_2 sequestration, along with enhanced tobacco seed production, following foliar application of the CeO_2 + 50 mM[Cho][Asc] nanoformulation compared to the control treatment. CeO_2 + [Cho][Asc] nanoformulation promotes additional CO_2 sequestration of 1.3–1.6 t/hectare compared to CeO_2 and IL treatments, suggesting that both CeO_2 and IL have a synergistic effect in mitigating the effects of climate change. While the potential of IL-modified CeO_2 to promote plant growth and CO_2 sequestration with potential for large-scale application is evident, the study recognizes the need for further research to understand plant-nanoformulation interactions at the plant molecular level, to test the suitability of this nanoformulation for other plant species, and to assess toxicity for large-scale application.

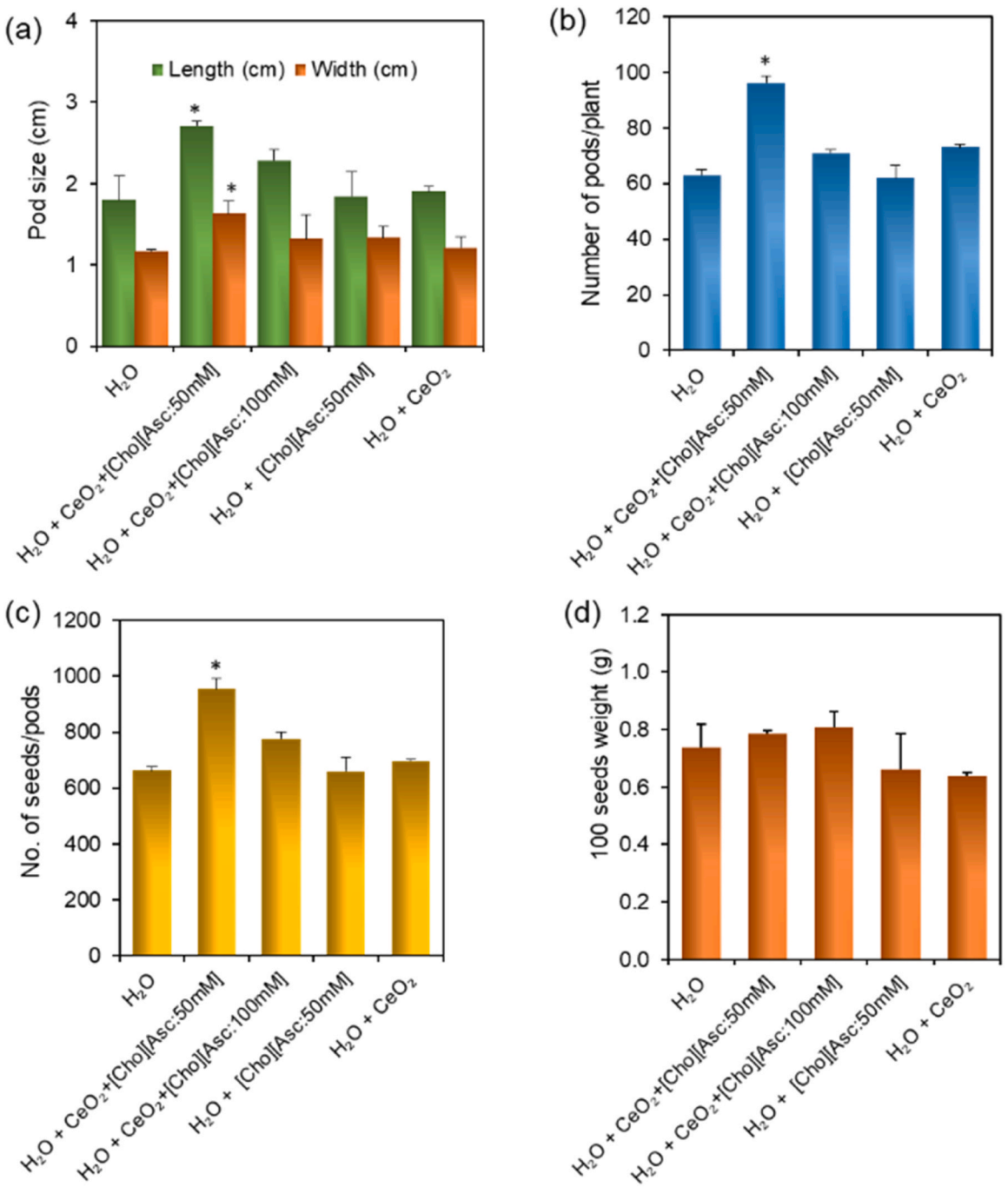

Fig. 7. Assessment of yield performance in tobacco plants based on pod size (a), number of pods per plant (b), number of seed per (c), and 100 seeds weight following treatment with IL-modified nanoceria. Error bars represent the standard error of the mean (SEM), and (*) indicates statistically significant differences ($p < 0.05$) as compared to the control..

CRediT authorship contribution statement

Dibyendu Mondal: Writing – original draft, Visualization, Validation, Supervision, Conceptualization. **Coutinho João:** Writing – review & editing, Validation, Formal analysis. **Gregory Franklin:** Writing – review & editing, Validation, Project administration, Funding acquisition. **Kiirika Leonard:** Writing – review & editing, Visualization, Methodology, Formal analysis, Data curation. **Martins Mónia:** Writing – review & editing, Methodology, Investigation, Formal analysis, Data curation. **Lakshmipathy Muthukrishnan:** Writing – review & editing, Formal analysis, Data curation. **Shaoo Suman:** Writing – review & editing, Methodology, Formal analysis, Data curation. **Dawid Perlikowski:** Writing – review & editing, Formal analysis, Data curation. **Nicolas Schaeffer:** Writing – review & editing, Investigation, Formal analysis, Data curation.

Declaration of Competing Interest

The authors declare that they have no known competing financial interests or personal relationships that could have appeared to influence the work reported in this paper.

Acknowledgments

This work was supported by the NANOPLANT project, which received funding from the European Union's Horizon 2020 research and innovation program under grant agreement no. 856961 NANOPLANT. This work was partly developed within the scope of the project CICECO-Aveiro Institute of Materials, UIDB/50011/2020, UIDP/50011/2020 and LA/P/0006/2020, CIMO, UIDB/00690/2020 (DOI: 10.54499/UIDB/00690/2020) and UIDP/00690/2020 (DOI: 10.54499/UIDP/00690/2020); and SusTEC, LA/P/0007/2020 (DOI: 10.54499/LA/P/0007/2020) financed by national funds through the FCT/ MCTES (PIDDAC).

Appendix A. Supporting information

Supplementary data associated with this article can be found in the online version at doi:10.1016/j.indcrop.2025.122609.

Data availability

Data will be made available on request.

References

Abbas, Q., Liu, G., Yousaf, B., Ali, M.U., Ullah, H., Munir, M.A.M., Ahmed, R., Rehman, A., 2020. Biochar-assisted transformation of engineered-cerium oxide nanoparticles: effect on wheat growth, photosynthetic traits and cerium accumulation. Ecotoxicol. Environ. Saf. 187, 109845. https://doi.org/10.1016/j.ecoenv.2019.109845.

Ahmad, S., Sehrish, A.K., Ai, F., et al., 2024. Morphophysiological, biochemical, and nutrient response of spinach (Spinacia oleracea L.) by foliar CeO2 nanoparticles under elevated CO2. Sci. Rep. 14, 25361. https://doi.org/10.1038/s41598-024-76875-z.

Ahmad, S., Sehrish, A.K., Tabassam, R., Ai, F., Naeem, M.K., Jamil, A., Ali, S., Guo, H., 2025. Nutrient strengthening and stress alleviation in rice (Oryza sativa L.) via foliar ceria nanoparticles and biochar amendment under elevated CO2-mediated warming. Plant Physiol. Biochem 229, 110364. https://doi.org/10.1016/j.plaphy.2025.110364.

Aresta, M., Dibenedetto, A., Angelini, A., 2014. Catalysis for the valorization of exhaust carbon: a key issue for sustainable energy. Chem. Rev. 114, 1709–1742. https://doi.org/10.1021/cr4002758.

Blöchl, P.E., 1994. Projector augmented-wave method. Phys. Rev. B Condens. Matter 50, 17953–17979. https://doi.org/10.1103/PhysRevB.50.17953.

Chandra, S., Pradhan, S., Mitra, S., Patra, P., Bhattacharya, A., Pramanik, P., Goswami, A., 2014. High throughput electron transfer from carbon dots to chloroplast: a rationale of enhanced photosynthesis. Nanoscale 6, 3647–3655. https://doi.org/10.1039/C3NR06079A.

Daneshvar, E., Wicker, R.J., Show, P.-L., Bhatnagar, A., 2022. Biologically-mediated carbon capture and utilization by microalgae towards sustainable CO2 biofixation and biomass valorization – A review. Chem. Eng. J. 427, 130884. https://doi.org/10.1016/j.cej.2021.130884.

Du, W., Gardea-Torresdey, J.L., Ji, R., Yin, Y., Zhu, J., Peralta-Videa, J.R., Guo, H., 2015. Physiological and biochemical changes imposed by CeO_2 nanoparticles on wheat: a life cycle field study. Environ. Sci. Technol. 49, 11884–11893. https://doi.org/10.1021/acs.est.5b03055.

Feng, Y., Wang, C., Chen, F., Cao, X., Wang, J., Yue, L., Wang, Z., 2022. Molecular mechanisms of CeO_2 nanomaterials improving tomato yield, fruit quality, and postharvest storage performance. Environ. Sci. Nano 9, 4382–4392. https://doi.org/10.1039/D2EN00783E.

Gan, Y., Liang, C., Chai, Q., Lemke, R.L., Campbell, C.A., Zentner, R.P., 2014. Improving farming practices reduces the carbon footprint of spring wheat production. Nat. Commun. 5, 5012. https://doi.org/10.1038/ncomms6012.

Giraldo, J.P., Landry, M.P., Faltermeier, S.M., McNicholas, T.P., Iverson, N.M., Boghossian, A.A., Reuel, N.F., Hilmer, A.J., Sen, F., Brew, J.A., Strano, M.S., 2014. Plant nanobionics approach to augment photosynthesis and biochemical sensing. Nat. Mater. 13, 400–408. https://doi.org/10.1038/nmat3890.

Gong, X., Hong, M., Wang, Y., Zhou, M., Cai, J., Liu, C., Gong, S., Hong, F., 2011. Cerium relieves the inhibition of photosynthesis of maize caused by manganese deficiency. Biol. Trace Elem. Res 141, 305–316. https://doi.org/10.1007/s12011-010-8716-z.

Jahani, S., Saadatmand, S., Mahmoodzadeh, H., Khavari-Nejad, R.A., 2019. Effect of foliar application of cerium oxide nanoparticles on growth, photosynthetic pigments, electrolyte leakage, compatible osmolytes, and antioxidant enzyme activities of Calendula officinalis L. Biologia 74 (9), 1063–1075. https://doi.org/10.2478/s11756-019-00239-6.

Jiménez-Rosado, M., Perez-Puyana, V., Guerrero, A., Romero, A., 2022. Micronutrient-controlled-release protein-based systems for horticulture: Micro vs. nanoparticles. Ind. Crops Prod. 185, 115128. https://doi.org/10.1016/j.indcrop.2022.115128.

Kaczmarek, D.K., Pacholak, A., Burlaga, N., Wojcieszak, M., Materna, K., Kruszka, D., Dąbrowski, P., Sobańska, K., Kaczorek, E., 2023. Dicationic herbicidal ionic liquids comprising two active anions for sustainable plant protection. ACS Sustain. Chem. Eng. 11, 13282–13297. https://doi.org/10.1021/acssuschemeng.3c02286.

Kresse, G., Furthmüller, J., 1996. Efficient iterative schemes for ab initio total-energy calculations using a plane-wave basis set. Phys. Rev. B 54, 11169. https://doi.org/10.1103/PhysRevB.54.11169.

Kresse, G., Joubert, D., 1999. From Ultrasoft Pseudopotentials to the Projector Augmented-Wave Method. Phys. Rev. B 59, 1758–1775. https://doi.org/10.1103/PhysRevB.59.1758.

Liu, S., Han, J., Ma, X., Zhu, X., Qu, H., Xin, G., Huang, X., 2024. Repeated release of cerium oxide nanoparticles altered algal responses: Growth, photosynthesis, and photosynthetic gene expression. EcoEnviron. Health 3, 290–299. https://doi.org/10.1016/j.eehl.2024.04.002.

Liu, Y., Liu, D., Han, X., Chen, Z., Li, M., Jiang, L., Zeng, J., 2024. Magnesium doped carbon quantum dot nanomaterials alleviate salt stress in rice by scavenging reactive oxygen species to increase photosynthesis. ACS Nano 18 (45), 31188–31203. https://doi.org/10.1021/acsnano.4c09001.

Lowry, G.V., Avellan, A., Gilbertson, L.M., 2019. Opportunities and challenges for nanotechnology in the agri-tech revolution. Nat. Nanotechnol. 14, 517–522. https://doi.org/10.1038/s41565-019-0461-7.

Ma, C., Borgatta, J., Hudson, B.G., Tamijani, A.A., Torre-Roche, R.D.L., Zuverza-Mena, N., Shen, Y., Elmer, W., Xing, B., Mason, S.E., Hamers, R.J., JC, White, 2020. Advanced material modulation of nutritional and phytohormone status alleviates damage from soybean sudden death syndrome. Nat. Nanotechnol. 15, 1033–1042. https://doi.org/10.1038/s41565-020-0776-1.

Martins, M.A.R., Kiirika, L.M., Schaffer, N., Sajnóg, A., Coutinho, J.A.P., Franklin, G., Mondal, D., 2024. Advances in sustainable resource management: recent developments and future perspectives. ACS Sustain. Resour. Manag. 1, 1291–1301. https://doi.org/10.1021/acssusresmgt.4c00041.

Matthews, M.L., 2023. Engineering photosynthesis, nature's carbon capture machine. PLoS Biol. 21 (7), e3002183. https://doi.org/10.1371/journal.pbio.3002183.

Maxwell, K., Johnson, G.N., 2000. Chlorophyll fluorescence—a practical guide. J. Exp. Bot. 51, 659–668. https://doi.org/10.1093/jexbot/51.345.659.

Momma, K., Izumi, F., 2008. VESTA: a three-dimensional visualization system for electronic and structural analysis. May 2008, doi: urnissn00218898 41 (3), 653–658. https://doi.org/10.1107/S0021889808012016.

Murashige, T., Skoog, F., 1962. A Revised Medium for Rapid Growth and Bio Assays with Tobacco Tissue Cultures. Plant Physiol. 15, 473–497. https://doi.org/10.1111/j.1399-3054.1962.tb08052.x.

Nuccio, M.L., McNeil, S.D., Ziemak, M.J., Hanson, A.D., Jain, R.K., Selvaraj, G., 2000. Choline import into chloroplasts limits glycine betaine synthesis in tobacco: analysis of plants engineered with a chloroplastic or a cytosolic pathway. Metab. Eng. 2, 300–311. https://doi.org/10.1006/mben.2000.0158.

Patel, A.K., Sumathi, Y., Singhania, R.R., Chen, C.W., Michaud, P., Dong, C.D., 2025. Innovative graphene quantum dots applications for enhancing lutein biosynthesis in microalgae biorefineries. Chem. Eng. J. 505, 159744. https://doi.org/10.1016/j.cej.2025.159744.

Peng, C., Ren, X., Khan, A., Chen, K., Gao, H., Ma, X., 2025. Insights into leaf morphology, photosynthetic efficiency, and light adaptation in cigar tobacco as light intensity transitions: A comprehensive analysis of transcriptomic, hormonal, and physiological responses. Ind. Crops Prod. 230, 121087. https://doi.org/10.1016/j.indcrop.2025.121087.

Perdew, J.P., Burke, K., Ernzerhof, M., 1996. Generalized Gradient Approximation Made Simple. Phys. Rev. Lett. 1996 (77), 3865–3868. https://doi.org/10.1103/PhysRevLett.77.3865.

Rossi, L., Zhang, W., Lombardini, L., Ma, X., 2016. The impact of cerium oxide nanoparticles on the salt stress responses of Brassica napus L. Environ. Pollut. 219, 28–36. https://doi.org/10.1016/j.envpol.2016.09.060.

Safat, S., Buazar, F., Albukhaty, S., Matroodi, S., 2021. Enhanced sunlight photocatalytic activity and biosafety of marine-driven synthesized cerium oxide nanoparticles. Sci. Rep. 11, 14734. https://doi.org/10.1038/s41598-021-94327-w.

Sanna, A., Uibu, M., Caramanna, G., Kuusik, R., Maroto-Valer, M.M., 2014. A review of mineral carbonation processes: achievements and challenges. Chem. Soc. Rev. 43, 8049–8080. https://doi.org/10.1039/C4CS00035H.

Servin, A.D., White, J.C., 2016. Nanotechnology in agriculture: Next steps for understanding engineered nanoparticle exposure and risk. NanoImpact 1, 9–12. https://doi.org/10.1016/J.IMPACT.2015.12.002.

Sharma, M., Mondal, D., Sequeira, R.A., Talsaniya, R.K., Maru, D.A., Moradiya, K., Prasad, K., 2021. Syntheses and characterization of few bio-ionic liquids comprising of cholinium cation and plant derived carboxylic acids as anions. J. Indian Chem. Soc. 98, 100205. https://doi.org/10.1016/j.jics.2021.100205.

Shen, M., Guo, W., Tong, L., Wang, L., Chu, P.K., Kawi, S., Ding, Y., 2025. Behavior, mechanisms, and applications of low-concentration CO_2 in energy media. Chem. Soc. Rev. 54, 2762–2831. https://doi.org/10.1039/D4CS00574K.

Witmer, J.R., Wetherell, B.J., Wagner, B.A., Du, J., Cullen, J.J., Buettner, G.R., 2016. Direct spectrophotometric measurement of supra-physiological levels of ascorbate in plasma. Redox Biol. 8, 298–304. https://doi.org/10.1016/j.redox.2016.02.004.

Wu, H., Tito, N., Giraldo, J.P., 2017. Anionic cerium oxide nanoparticles protect plant photosynthesis from abiotic stress by scavenging reactive oxygen species. ACS Nano 11 (11), 11283–11297. https://doi.org/10.1021/acsnano.7b05723.

Xia, Y., Liu, D., Dong, Y., Chen, J., Liu, H., 2018. Effect of ionic liquids with different cations and anions on photosystem and cell structure of Scenedesmus obliquus. Chemosphere 195, 437–447. https://doi.org/10.1016/j.chemosphere.2017.12.054.

Yan, Y., Wu, S., Kang, S., Amin, S.E., Cheng, S., Wang, F., 2025. Mn_3O_4 nanozyme-based nanofertilizer for plant acclimation to a combination of drought and cadmium stresses. Chem. Eng. J. 519, 165545. https://doi.org/10.1016/j.cej.2025.165545.

Yu, F., Zhou, Y., Cao, K., Gao, W., Gao, B., Sun, L., Liu, S., Wang, L., Ding, Y., 2018. Phytotoxicity of ionic liquids with different structures on wheat seedlings and evaluation of their toxicity attenuation at the presence of modified biochar by adsorption effect. Chemosphere 196, 331–338. https://doi.org/10.1016/j.chemosphere.2017.12.148.

Ze, Y., Liu, C., Wang, L., Hong, M., Hong, F., 2011. The regulation of TiO_2 nanoparticles on the expression of light-harvesting complex II and photosynthesis of chloroplasts of Arabidopsis thaliana. Biol. Trace Elem. Res 143 (2), 1131–1141. https://doi.org/10.1007/s12011-010-8901-0.

Zibordi-Besse, L., Seminovski, Y., Rosalino, I., Guedes-Sobrinho, D.D., Da Silva, J.L.F., 2018. Physical and Chemical Properties of Unsupported (MO2)n Clusters for M = Ti, Zr, or Ce and n = 1–15: A Density Functional Theory Study Combined with the Tree-Growth Scheme and Euclidean Similarity Distance Algorithm. J. Phys. Chem. C. 122, 27702–27712. https://doi.org/10.1021/acs.jpcc.8b08299.